BEND-STRENGTH OF NOVEL FILAMENT WOUND SHEAR REINFORCEMENT

Saverio Spadea*, John Orr, Kristin Ivanova

Department of Architecture and Civil Engineering

University of Bath

Claverton Down, BA2 7AY, Bath (United Kingdom)

*corresponding author: s.spadea@bath.ac.uk

Abstract

The winding of Fibre Reinforced Polymer (FRP) tows around longitudinal reinforcing bars provides a novel method for the fabrication of reinforcement cages for concrete structures. A key limitation on the contribution of FRP to the shear capacity of a concrete member is found at corners, where stress concentrations can lead to premature failure. An experimental programme, comprising 30 test samples, was undertaken to assess the bend capacity of filament wound FRP (W-FRP) shear links manufactured using a carbon tow impregnated with epoxy resin. A new methodology was developed to allow for rapid testing of the samples as well as their self-re-alignment during load application. A fixed bend radius of 5mm and six non-circular fibre cross sectional areas having different width-thickness ratios were considered. Additionally, 18 samples were tested to measure the tensile properties of the straight reinforcement. The results indicate that W-FRP exhibit improved bend strength as compared to conventional FRP with circular sections, as a larger width-thickness ratio of the reinforcement provided more strength for a given cross sectional area. A good correlation between the test results and predictions of the W-FRP bend strength was observed when the specimens were modelled as a collection of transformed individual circular sections.

Keywords

Carbon fibre; Mechanical testing; Filament winding; W-FRP.

1 Introduction

Optimising the cross-section of reinforced concrete elements, by tailoring their shear and bending capacities at every cross-section to withstand the applied load can result in material savings of up to 40% [1]. During this process, the self-weight of the structural elements is reduced, leading to lower material costs. However, such optimised sections are often non-prismatic, creating practical and technical issues associated with reinforcement cages.

Reinforcement solutions utilising traditional steel shear links are hard to achieve in non-prismatic sections due to construction costs and practicality issues [2]. Subsequently, Fibre reinforced polymers (FRP) reinforcement has received a lot of attention, as the flexibility of the raw fibres prior to the application of resin allows reinforcement to be shaped precisely as required [3]. FRP also has a number of physical advantages over steel: it is non-magnetic, has a very high strength to weight ratio, and is not susceptible to corrosion [4, 5].

A complication with FRP shear reinforcement is its linear stress-strain behaviour and anisotropic properties. Bends in shear reinforcement, which help to develop sufficient anchorage with the concrete, are associated with additional stress concentrations: transverse stresses due to bearing on the concrete; longitudinal stresses along the length of the fibres due to tensile forces in the shear reinforcement; and kinking of the inner fibres due to the bend generation during manufacture As FRPs do not yield, the combination of these three factors creates an intrinsically weak point at the corners of the reinforcing cage. Bend strength capacities as low as 30-40% of the tensile strength in the

direction of the fibres are often reported for FRP stirrups with circular cross section [6-10]. As a consequence, strength of the bend governs the capacity of FRP shear reinforcement.

It has recently been suggested that the use of FRP stirrups with a rectangular cross sections and large width-to-thickness ratio can result in a bend strength up to 76% of the tensile strength of a straight portion of FRP, due to the lower number of kinked fibres at corners achieved by reducing the difference between the outer and the inner radius [8]. Another major parameter reported to affect the bend strength of FRPs are ratio between radius of bend and bar diameter.

Techniques such as filament winding, which is often used in aeronautical engineering, can be applied to wind fibres coated in resin around longitudinal reinforcement bars to create reinforcement cages for concrete structures (Figure 1). Complex geometries of internal reinforcement can be fabricated using this technique, a particular advantage for the construction of optimised concrete beams. Moreover, the winding process forms the fibres in wide and thin cross sections, the ideal geometry identified by Lee *et al.* [8],[11]. This method also allows for quick and accurate fabrication of reinforcement cages with consistent quality. Traditional FRP stirrups are made by bending pultruded bars prior to full polymerization of the resin. The filament winding technique allows the radius of curvature of the bend to be tighter than for traditional open stirrups as the fibres do not need to slide over each other as is required when bending a straight pultruded bar before the resin polymerizes

In the majority of FRP design codes, the shear capacity of flexural members is normally divided into contributions from the concrete and reinforcement [12]. A limiting factor in the contribution of the reinforcement is the strength of the FRP at the corners.

In this paper, the performance of filament wound CFRP shear links of a realistic size are investigated. The specimens tested simulate a slice of the optimised T-beam web recently tested by the same research group [13, 14] and including a combination of shear and longitudinal reinforcement. As filament winding was used to create the test samples, the corner radius of the shear links was determined by the diameter of the longitudinal reinforcement. The bend radius was therefore kept constant, with the variable investigated being a change in the number of wound layers. It is expected that as cross-sectional area increased the failure capacity of the link increases proportionally. However, when the cross-sectional area is increased, it is anticipated that there will be a larger volume of kinked fibres on the inside surface, resulting in a lower bend strength at failure. Tests were also performed on straight samples to measure the tensile properties of the W-FRP reinforcement. Experimental results are compared to theoretical predictions made using the guidance provided in ACI 440.1R [15] and a predictive equation proposed by Lee *et al.* [8]. The suitability of applying the test methodology to future local bend strength investigations is also reviewed.

2 Materials and predictions

2.1 Manufacturing

The W-FRP reinforcement was manufactured using an automated filament winding technique, which consist on wrapping continuous fibres under tension over a rotating mandrel. Although this method of fabrication has recently been proposed to create reinforcement cages for concrete structures [13, 14, 16], it is generally used to produce continuous hollow shapes with constant cross section.

Four #3 CFRP reinforcing bars [17] were attached longitudinally to the mandrel to form the corners of an idealized prism. The CFRP bars, having 10 mm diameter, aim to simulate

97 the longitudinal reinforcement of a realistic concrete beam during the manufacturing of W-
98 FRP cages. A refined system of control was employed to wind one or more carbon fibres
99 layers impregnated with resin. The carbon fibres are wound around the bars in the form of
100 closed rectangular stirrups with curved corners (bending radius, r_b, equal to 5 mm), a
101 process very similar to the one employed to produce optimized reinforcement cages.

102 **2.2 Tensile properties predictions**

103 A continuous 50k carbon fibre tow with a 240 GPa modulus of elasticity and a two-
104 component epoxy were employed. This class of epoxy resin is applied at room
105 temperature and is air cured, both considerable advantages for this application. A
106 summary of the properties of the raw materials and the estimated characteristics of the
107 final composite are reported in Table 1.

108 As the component densities are known, the resin content was determined by weighing
109 reinforcement of known length, subtracting the weight of fibres employed (based on fibre
110 volume and density) and converting the value into a volume. A consistent fibre-to-resin
111 volume-fraction-ratio of 0.45/0.55 (VF_f / VF_r) was observed.

112 Under the assumption of all fibres stressed uniformly up to failure and negligible
113 contribution of the resin, the expected tensile capacity of the reinforcement $f_{u,WFRP}$ is
114 computed as:

$$f_{u,WFRP} = \frac{f_{u,f}}{A_{WFRP}} A_f, \tag{1}$$

115 where $f_{u,f}$ and A_f are the tensile strength and the cross section of the carbon fibre tow,
116 respectively, whereas A_{WFRP} is the cross section of the whole WFRP (fibre tow and resin).
117 The expected modulus of elasticity in the direction of fibres is computed according to the
118 mixture law, assuming that all fibres are perfectly straight and aligned:

$$E_{CFRP} = VF_f \cdot E_f + VF_r \cdot E_r, \quad (2)$$

where E_f is the Modulus of elasticity of the fibres and E_r is the Modulus of elasticity of the resin.

Knowing the modulus of elasticity and tensile strength, and assuming a linear elastic behaviour up to failure, the expected ultimate strain of the composite, ε_u, is finally computed as:

$$\varepsilon_u = \frac{f_{u,WFRP}}{E_{CFRP}}. \quad (3)$$

All these predictions assume perfect fibres alignment and uniform stresses in the different fibres, which will inevitably result in an overestimation of the mechanical properties of the composite.

2.3 Bent corners strength predictions

Two methods of predicting the strength of the links at bends, $f_{fb,WFRP}$, were used in this study: ACI 440.1R [15] formula, shown in Equation (4), and a method proposed by Lee *et al.* [8], Equation (6).

As the cross sections of the shear links tested in this investigation are not circular, the equation proposed by ACI 440.3R [18] for calculating an equivalent section diameter (d_b) was used in combination with the equation proposed by ACI 440.1R [15]:

$$f_{fb,WFRP} = (0.05\frac{r_b}{d_b} + 0.3) \cdot f_{fu,WFRP} \le f_{fu,WFRP}, \quad (4)$$

where

$$d_b = 2\sqrt{\frac{A_{WFRP}}{\pi}}. \quad (5)$$

Lee *et al.* [8] proposed a revised equation for estimating the bend strength accounting for reinforcement with rectangular cross section:

$$f_{fb,WFRP} = (0.02\frac{r_b}{d_{fi}} + 0.47) \cdot f_{fu,WFRP} \leq f_{fu,WFRP}, \quad (6)$$

where d_{fi} pertains to a different definition of equivalent diameter of the reinforcement,

$$d_{fi} = \frac{2}{\sqrt{\pi}} t_f. \quad (7)$$

This latter equation is obtained by representing the rectangular cross section with a collection of small circular sections, whilst still retaining the correct number of kinked fibres [8].

Current guidance regarding detailing of shear reinforcement provided by{ACI 440.1R, 2015 #9, suggests a minimum ratio of bend radius to diameter of FRP of three or more to avoid premature shear failure at the bends, following research done by Ehsani *et al.* [19]. During filament winding the diameter of the longitudinal reinforcement determines that radius of the bend, therefore the bend ratios of 5mm tested in this investigation are much lower than these recommendations, as they were designed to represent a realistic combination of longitudinal and shear reinforcement.

It is important to note that both calculation methods result in a fixed constant that determines the minimum proportion of the tensile strength of the straight portion utilised at the bend. ACI 440.1R [15] suggests a proportion of 0.3, so the bend strength should be a minimum of 30% of the tensile strength of the straight portion. On the other hand [8] recommends a minimum of 47%.

3 Test Methodology

Tensile tests (Series T) and corner tests (Series L) were undertaken to inform the design and analysis of optimised beam specimens reinforced with W-FRP:

- Series T: Tensile tests are aimed at the determination of the modulus of elasticity and strength of straight W-FRP
- Series L: Push-off tests are aimed at the determination of strength of W-FRP at bends and the corresponding ultimate strains.

In both series of tests, six different fibre contents were taken in consideration, varying the number of the over-posed layers of carbon fibre tow from a minimum of one to a maximum of six. Table 2 shows the nominal cross sectional properties of the samples. The average thickness, t_{WFRP}, is measured at the reinforcement bends, whereas the width, w_{WFRP}, is conventionally computed known the total area, A_{WFRP}, and assuming a rectangular cross section. An overview of the test program, including the number of repeats, is also shown in Table 2.

3.1 Tensile tests

EN ISO 527-1 [20] and EN ISO 527-5 [21] describe the reference test method for the determinations of tensile properties of unidirectional FRP composites. According to these, a 150 mm clear distance was adopted between tabs used as grips. The width and the overall length of the samples were not, however, compliant with the standards. The reinforcement width was determined by the natural spread of the 50k carbon tow during the winding process, which is affected by the number of over-posed layers. The design of an effective gripping system - an updated version of the test method employed in [16] - includes several features aimed at avoiding slip or damage of the samples during testing. It resulted in a 500mm overall length of the specimen, in contrast to the 250mm overall length prescribed by the standards. The details of the specimens along with the gripping system are shown in Figure 2.

179 Eighteen straight samples with short curved ends were therefore cut from W-FRP
180 rectangular closed stirrups (internal dimensions: 500mm × 45mm). At the winding stage,
181 a layer of carbon fabric impregnated with epoxy resin was attached on both faces of the
182 two ends of the specimen, for a length of 175 mm, leaving required test clear length of
183 150 mm. This was done, in the first instance, to improve the mechanical properties of the
184 reinforcement at anchorages and prevent undesired modes of failure. As two couples of
185 aluminium tabs with channel cross section were bonded on the strengthened zones, the
186 carbon fabric resulted also in enhancing the effectiveness of the adhesive connection. The
187 175mm long channel tabs were specifically designed with purpose of accommodating the
188 cross section of the reinforcement and the strengthening fabric with a 1mm layer of
189 adhesive on each adherent surface. Edges of 2mm at the sides of the tabs were used to
190 prevent crushing of the specimens. The inner surface of each aluminium channel was
191 engraved with transverse notches and thoroughly degreased before applying a 1 mm layer
192 of two-component epoxy paste adhesive, being fastened to the specimens with clamps
193 and left to cure. It should be noted that additional slip resistance was provided by the
194 corner at the ends of the specimens, having been set up in contrast to the aluminium ends.
195 The mid-section of each specimen was instrumented with a uniaxial strain gauge having
196 6 mm gauge length bonded onto one face of the carbon strip. In order to improve the
197 adhesive joint performance, a pressure of 10 MPa was passively applied on the first 75
198 mm portion of the aluminium tabs controlling the screwing torque on a system of metallic
199 clamps. The specimens were gripped in the testing machine with a pressure of 20 MPa
200 on end portion of the aluminium tabs. The gripping system adopted allows the level of
201 pressure applied to the aluminium tabs to be controlled and differentiated along the
202 specimen length. The tests were performed in displacement control at 1.0 mm/min.

3.2 Bent corners tests

Both ACI 440.3R [18] and CSA S806 [22] adopt a similar test method for FRP bend strength (Figure 3a), in which large sample sizes are used to test realistic FRP stirrups. In contrast, W-FRP technology allows for diffuse shear reinforcement in structurally optimised thin walled concrete sections, with the combination of the two resulting in a relevant scale difference in the required reinforcement cross sections and overall geometry. Because the WFRP is so thin in comparison to a pultruded bar, tests on W-FRP links performed per conventional methods are likely to be affected by imperfections in test procedures and sample quality such as eccentricities. There also remains an uncertainty regarding how the scale difference between the samples tested and section used in beams affects the behaviour of the bend.

A new test procedure was developed with the aim of producing an adaptable small scale bend strength test methodology. The test procedure draws inspiration from the artificial crack test approach used by Ueda *et al.* [23] and Ishihara *et al.* [24] (Figure 3b). The resulting set-up forms a gravity reliant tension system, allowing for self-alignment in the case of small sample eccentricities, which in turn mitigates the concerns regarding eccentric loading leading to premature failure. In addition, longitudinal reinforcement is placed in the corners of the shear links, creating a more realistic model of stress concentrations at the bends. The sample configuration used in the present investigation, shown in Figure 4, aims to be a close representation of a slice through the web of an optimised reinforced concrete beam. The internal dimensions of the shear links tested are 45mm wide and 260mm deep. The same bars used during the winding process (#3 CFRP) are cut at 100mm length and used to simulate the effect of longitudinal reinforcement. A 3mm acrylic plate is cast in the centre of concrete specimens, separating the specimen in

two halves and consequently creating an artificial crack which can widen following load application. The acrylic plate has openings to accommodate the shear link passing between the two concrete halves. Two steel circular hollow sections are cast in each half of the specimen, directly adjacent to the 3mm acrylic plate, to allow for load application. The samples incorporates carbon fibre spirals, installed in each half of the concrete samples perpendicular to the load application, to ensure concrete confinement.

During the sample preparation, one half of each link was de-bonded from the centre of the sample to the start of the bend using non-drying modelling clay. This was intended to eliminate friction and interlock between the CFRP and the concrete with the aim to evaluate the bend capacity only, excluding any strength contribution due to the FRP-to-concrete bond. Due to the manufacturing method, each shear link ends up with a collection of continuous layers on one side and with overlapped layers on the other side (the ends of first and the last carbon tow layer). Since the debonded side is the one effectively subject to the bend test, the non-drying modelling clay was purposely applied on the continuous side of the stirrups. The samples were instrumented with two uniaxial strain gages (USG-A and USG-B), installed at mid-length of the two braces of the stirrups, as shown in Figure 4 (front view).

The test specimens were cast in plywood formwork. To aid the positioning of the steel tubes and the longitudinal acrylic bars connected to the shear link, grooves of the correct size and location are cut into the base of each mould. A C30/37 concrete class with maximum aggregate size of 10mm and S4 slump was employed. During casting, the samples were vibrated to ensure compaction of the concrete.

The 2-part loading rig shown in Figure 5 was used for the load application during testing. The two external clamps were made from 12mm and 20mm S275 steel plates, for the

vertical and horizontal member respectively. M20 grade 8.8 bolts connected the external clamp sections and the test sample, by slotting in the cast-in steel tube.

When positioned in the loading machine, the samples were allowed to self-align, through the embedded tubes which provide an axis of rotation. During the load tests, a pre-load of 0.3 kN was applied to the specimen, followed by a smooth displacement rate of 1mm per minute, until failure. Strains, applied load and displacement were measured during the experiment.

The effect of change in cross sectional area and aspect ratio with a constant bend radius of 5mm were investigated. Six cross sectional areas were tested: 1, 2, 3, 4, 5, and 6 layers of 50k filaments carbon fibre tow. As advised by ACI 440.3R [18], five specimens were tested for each cross section change, to review the consistency of the results.

4 Results and Discussion

4.1 Tensile Tests

Figure 6 shows the typical failure mode observed during tensile tests. As expected, the ruptures were sudden and brittle, showing clear delamination of fibres from the epoxy matrix.

Table 3 summarises the results obtained through the tensile tests (full data can be viewed in the data archive, see data access statement for details). The 25% and the 50% of the failure load ($F_{25\%}$ and $F_{50\%}$, respectively) and corresponding values of strains ($\varepsilon_{25\%}$ and $\varepsilon_{50\%}$, respectively) are identified for each tested samples. The modulus of elasticity was computed according to the procedure suggested in Annex C of CSA S806 [22]:

$$E_{WFRP} = \frac{F_{50\%} - F_{25\%}}{A_{WFRP}(\varepsilon_{50\%} - \varepsilon_{25\%})}. \quad (8)$$

272 Knowing the failure load (F_u) and the modulus of elasticity (E_u), the ultimate strain
273 exhibited by each specimen is computed, assuming a linear elastic behaviour for the
274 material, as:

$$\varepsilon_u = \frac{F_u}{E_u A_{WFRP}}. \quad (9)$$

275 The ultimate strain is purposely not identified by the strain readings at ultimate load, since
276 the measurements may be unreliable at failure, due to uneven damage of the specimens.
277 The mean value, the standard deviation and the coefficient of variance are reported in
278 Table 3 for the experimental variables obtained on each set of tests, with statistics
279 showing good consistency (CoV always below 10%). Experimental values of the ultimate
280 stress detected are systematically lower than predicted values, confirming that bundle
281 theory has a large effect on tensile capacity of FRP [25].
282 The mean values of failure loads and modulus of elasticity obtained on different set of
283 samples against the number of layers composing the samples are reported in Figure 7 and
284 Figure 8, respectively. Figure 7 includes additional results obtained on 8 layers hand-
285 wound reinforcement [16] that was manufactured using the same materials. The best
286 fitting curves and the range error bars are also reported in the two plots for each set of
287 data. Figure 7 shows how the strength of straight reinforcement is not perfectly
288 proportional to the number of layers. The experimental data perfectly fit a parabolic curve
289 with intercept set to zero. It is known that the ultimate tensile stress tends to reduce due
290 as the cross sectional area of FRP elements increases to the requirement for the resin to
291 transmit stresses between fibres, although this effect is supposed to be appreciable for
292 large bar diameter [26]. This circumstance underlines that each successive layer of carbon
293 fibre that is added during the winding process results in being slightly less efficient than
294 the one previously wound. Figure 8 shows that this phenomenon has a major influence

295 on the modulus of elasticity, which is affected by the higher number of misaligned fibres
296 that naturally occur when adding a new layer upon the others. The modulus of elasticity
297 linearly decreases when increasing the number of layers, rather than remaining constant,
298 with a rate of 0.72 GPa per number of layer.

299 **4.2 Bent Corners Tests**

300 As discussed earlier, the test methodology for bent corners was designed so that the
301 samples could re-align when eccentricities were present. The time lapse of the load
302 application in Figure 9 shows the sample (Figure 9a) remaining perfectly aligned after
303 the two concrete blocks separate along the discontinuity created by the acrylic plate
304 (Figure 9b). A rotation between the two parts is only visible after the CFRP link failure
305 occurs (Figure 9c). Concrete cracking was not observed, indicating that the addition of
306 the CFRP reinforcement double spirals cages in the concrete blocks was effective in
307 confining the samples. The failure location was consistently detected at the bent portion
308 of the reinforcement on the de-bonded side of the samples. Of course, it was not possible
309 to check whether or not the failure was simultaneously happening on both legs as they
310 were embedded in concrete.

311 Table 4 below summarises the experimental results obtained (full data can be viewed in
312 the data archive, see data access statement for details). The following variables are taken
313 into consideration for each of the tested specimen:

314 - $F_{u,b}$ is the ultimate capacity exhibited by the sample, which includes the
315 contribution of two reinforcement legs;
316 - $\varepsilon_{u,b,ave}$ is the ultimate strain, computed as the average between the two strain gauge
317 observations at failure:

$$\varepsilon_{u,b,ave} = \frac{\varepsilon_{u,A} + \varepsilon_{u,B}}{2}; \quad (10)$$

318 - $\varepsilon_{u,b,\max}$ is the maximum ultimate strains between the two strain gauge observations
319 at failure:

$$\varepsilon_{u,b,\max} = \max(\varepsilon_{u,A}, \varepsilon_{u,B}). \quad (11)$$

320 The mean value (μ), the standard deviation (*SD*) and the coefficient of variance (*CoV*) of
321 these variables are calculated on the five samples populations for each of the fibre
322 contents considered.
323 Table 4 also reports the number of samples in which was possible to monitor the two
324 strains up to failure (ε_A and ε_B), as some of the gauges failed to produce signal before
325 the ultimate load was reached.
326 The failure load exhibited show good consistency, with coefficient of variation generally
327 lower than 10%. Only the six layer samples show a coefficient of variation of 11.2%.
328 Strain gauge data is more scattered, with measured strains at failure having maximum
329 *CoV* of 21.0% in the maximum value of strain ($\varepsilon_{u,b,\max}$, Set L1) and 23.2% in the average
330 value of strain ($\varepsilon_{u,b,ave}$, Set L2). The limited difference between the mean of average
331 ultimate strains and the maximum ultimate strains indicates that the load was quite equally
332 distributed between the two legs of the FRP links up to failure.
333 The mean values of failure loads obtained on different set of samples against the number
334 of layers composing the samples are reported in Figure 10. The best fitting curves and the
335 range error bars are also shown on the plot. Also in this case the experimental data
336 perfectly fit a parabolic curve with intercept set to zero (R^2=1). However, the non-linear
337 component of the curve is more relevant in comparison to the case of the straight
338 reinforcement.

4.3 Validation of results

As discussed earlier, two equations to relate bend strength to the strength of the equivalent straight reinforcement are available in literature. To aid comparisons, the experimental bend strength to tensile strength ratio was defined in relation to the known variables F_b and F_u:

$$f_{u,b}/f_u = \frac{F_b}{2 \cdot F_u}. \tag{12}$$

According to the approximated solution proposed by Hinkley [27], the ratio of the two normally distributed variables can be, under certain circumstances, still considered a normal distribution. The mean value is set equal to the ratio of the two mean values:

$$\mu(f_{u,b}/f_u) = \frac{\mu(f_{u,b})}{\mu(f_u)} = \frac{\mu(F_b)}{2 \cdot \mu(F_u)}, \tag{13}$$

whereas the standard deviation can be approximated as follows:

$$SD(f_{u,b}/f_u) = \mu^2(f_{u,b}/f_u) \cdot \left(CoV^2(f_{u,b}) + CoV^2(f_u)\right). \tag{14}$$

Table 5 shows the statistics of the experimental bend strength to experimental ultimate tensile strength ratio, f_b/f_u, for each set of specimens, as well as the predictions performed according to the ACI 440.1R [15] and Lee *et al.* [8] equations.

The coefficient of variations calculated for the six sets of samples show good reliability of the experimental results, with maximum scattering detected in the six-layer group of samples (*CoV* equal to 12.2%).

The one-layer samples reviewed in this work resulted in an average bend strength equal to 62% of the ultimate tensile strength of a straight portion. In contrast, the efficiency of corners expected into conventional stirrups with circular sections, according to ACI 440.1R [15], is only 41%.

358 A big drop in efficiency was shown by the two-layer samples, confirming that
359 successively over-posed tows have reduced mechanical performances. The average bend
360 strengths is, in this case, 50% of the ultimate tensile strength of a straight portion (-26%
361 with respect to the one layer samples). The six-layer samples exhibited the lowest
362 efficiency, resulting in an average bend strength of 45% of the tensile strength of the
363 straight portion (-38% with respect to the one-layer samples), whilst always showing bend
364 strengths higher than the expected in conventional stirrups with circular cross sections.
365 The increase in the number of layers not only causes a proportional increase of the cross-
366 sectional area but also a decrease of the width-to-thickness aspect ratio (w_{WFRP}/t_{WFRP}) of
367 the reinforcement (Table 2), which may be an additional cause of the reduced efficiency.
368 In fact, the use of a rectangular section that is wider and thinner can result in a lower
369 volume of kinked fibres for the same cross sectional area [8]. Whilst the one layer
370 reinforcement appears to be the most efficient, in many cases it could be impractical, as
371 it will result in a very closely wound reinforcement cage, which is likely to cause issue
372 with concrete casting. Figure 11 shows the experimental values of bends strength to
373 tensile strength ratio and the predictions performed according to the ACI 440.1R [15] and
374 Lee *et al.* [8] equations, against the number of WFRP layers composing the samples. The
375 values representing the 5% quantile of the normal distribution are also represented on the
376 same diagram.
377 The plot shows that the experimental results are always included between the bounds
378 outlined by the two models. The ACI 440.1R [15] underestimates the strength of bent
379 corners of the reinforcement whereas the equation proposed by Lee *et al.* [8]
380 overestimates it, whilst representing a closer match to the experimental values. A linear
381 regression analysis performed on the 5% quantile experimental data suggests that the 0.47

382 constant proposed by Lee *et al.* [8], equation (6), could be reduced to 0.34 for future use
383 on filament wound reinforcement prediction. This allows to obtain the following
384 predicting equation:

$$f_{fb,WFRP} = (0.02\frac{r_b}{d_{fi}} + 0.34) \cdot f_{fu,WFRP} \leq f_{fu,WFRP}, \quad (15)$$

385 having the same structure of equation (6), and an identical slope coefficient 0.02.
386 Therefore the equivalent diameter d_{fi}, defined according equation (7) only as function of
387 the thickness, t_{WFRP} , seems to properly relate the bent strength of the W-FRP
388 reinforcement with flat cross section to the tensile strength of an identical reinforcement.
389 Equation (15) cannot be considered a general result, due to the specific case study taken
390 into consideration. However, it can be applied for the design of wound reinforcement with
391 inner radius of curvature of bends, r_b, fixed to the value of 5 mm.

392 **Conclusions**

393 In this paper the bend strength of the recently developed filament wound FRP
394 reinforcement (W-FRP) was compared with those of the equivalent straight
395 reinforcement. The experimental investigation focused on the effects of increasing the
396 number of wound layers at 5mm bend radius, generally showing that filament winding
397 FRP shear reinforcement around the longitudinal reinforcement bars offers a consistent
398 fabrication procedure, whilst improving the mechanical behaviour of the shear
399 reinforcement compared to that of circular bars. In particular, the following conclusions
400 were drawn:

401 - The novel sample configuration and test method proposed provide an effective
402 and simple procedure to determine the bend strength of CFRP shear links,

allowing for the automatic re-alignment of the samples during testing and leading to extremely consistent results.

- Due to the increasing number of misaligned and/or kinked fibres, each successive over-posed layer of carbon fibre added during the winding process exhibited reduced mechanical performances (tensile strength, modulus of elasticity, bent corner strength).
- All the experimental results fell in the range between the two available predictions, with Lee *et al.* [8] providing an overestimation and the ACI 440.1R [15] providing an underestimation.
- An adapted equation for the design wound reinforcement with inner radius of curvature of bends fixed to the value of 5 mm was proposed.
- Due to the lower number of kinked fibres at corners achieved by reducing the difference between the outer and the inner radius the bent strength shown by filament wound reinforcement was systematically higher than the one expected into conventional stirrups with circular sections having same cross sectional area.
- A good correlation between the test results and predictions of the W-FRP bend strength was observed when sections were modelled as a collection of transformed individual circular sections, further validating the results of Lee *et al.* [8].

Following the results of this experimental study, especially regarding the success of the test methodology, there is scope for a wide range of future work. A larger study should be conducted incorporating the change of different parameters. A broader range of bend radii should be explored to review correlations that were not yet apparent. Furthermore, the results from the small individual bend strength tests should be reviewed against results from full sized beam tests. This will provide an insight of how realistic the small scale

tests are and what additional contribution to shear resistance is provided by the beam set-up. These studies will allow to the development of a simplified design equation able to predict the strength of FRP reinforcement at bent corners that will rely on a proper interpretation of the mechanical phenomenon.

Acknowledgements

This work is funded by the Engineering and Physical Sciences Research Council under grant EP/M01696X/1.

Data Access Statement

All data created during this research are openly available from the University of Bath data archive at http://doi.org/10.15125/BATH-00

References

[1] Orr, J.J., A.P. Darby, T.J. Ibell, and M.C. Evernden. *Innovative reinforcement for fabric formed concrete structures*. in *American Concrete Institute, ACI Special Publication*. 2011.

[2] Orr, J.J., T.J. Ibell, A.P. Darby, and M. Evernden, *Shear behaviour of non-prismatic steel reinforced concrete beams.* Engineering Structures, 2014. **71**: p. 48-59.

[3] Campbell, F.C., *Structural composite materials*. 2010, USA: ASM international. .

[4] Nanni, A., *Fiber-reinforced-plastic for concrete structures: Properties and applications*. 1993, Amsterdam: Elsevier Science.

[5] Ascione, L., G. Mancusi, and S. Spadea, *Flexural behaviour of concrete beams reinforced with GFRP bars.* Strain, 2010. **46**(5): p. 460-469.

[6] El-Sayed, A.K., E. El-Salakawy, and B. Benmokrane, *Mechanical and Structural Characterization of New Carbon FRP Stirrups for Concrete Members.* 2007.

[7] Ahmed, E.A., E. El-Salakawy, B. Benmokrane, and A.K. El-Sayed, *Bend Strength of FRP Stirrups: Comparison and Evaluation of Testing Methods.* 2010.

[8] Lee, C., M. Ko, and Y. Lee, *Bend Strength of Complete Closed-Type Carbon Fiber-Reinforced Polymer Stirrups with Rectangular Section.* Journal of Composites for Construction, 2014. **18**(1).

[9] Shehata, E., R. Morphy, and S. Rizkalla, *Fibre reinforced polymer shear reinforcement for concrete members: behaviour and design guidelines.* Canadian Journal of Civil Engineering, 2000. **27**(5): p. 859-872.

[10] Ascione, L., A.G. Razaqpur, and S. Spadea. *Effectiveness of FRP stirrups in concrete beams subject to shear*. in *7th International Conference on FRP Composites in Civil Engineering (CICE 2014)*. 2014.

[11] Lee, C., S. Lee, and S. Shin, *Shear Capacity of RC Beams with Carbon Fiber-Reinforced Polymer Stirrups with Rectangular Section.* Journal of Composites for Construction, 2016. **20**(4).

[12] Razaqpur, A.G. and S. Spadea, *Shear Strength of FRP Reinforced Concrete Members with Stirrups.* Journal of Composites for Construction, 2015. **19**(1).

[13] Spadea, S., J. Orr, and A. Nanni, *New frontiers for the use of FRP reinforcement in geometrically complex concrete structures*, in *Eight International Conference on Fibre-Reinforced Polymer (FRP) Composites in Civil Engineering*. 2016: Hong Kong.

[14] Spadea, S., J. Orr, T. Ibell, and A. Nanni, *Development of new FRP reinforcement for optimized concrete structures*, in *fib Symposium in 2017*. 2017: Mastricht, The Netherlands.

[15] ACI 440.1R, *Guide for the Design and Construction of Structural Concrete Reinforced with Fiber-Reinforced Polymer (FRP) Bars*. 2015, American Concrete Institute: Farmington Hills, MI.

[16] Spadea, S., J. Orr, Y. Yang, and A. Nanni, *Wound FRP shear reinforcement for concrete structures.* Journal of Composites for Construction, 2017.

[17] Hughes Brothers. *Aslan 200 Carbon Fiber Reinforced Polymer (CFRP) Bar - Product Data Sheet*. 2011; Available from: http://www.aslanfrp.com/Media/Aslan200_datasheet.pdf.

[18] ACI 440.3R, *Guide Test Methods for Fiber-Reinforced Polymers (FRPs) for Reinforcing or Strengthening Concrete Structures*. 2012, American Concrete Institute: Farmington Hills, MI.

[19] Ehsani, M.R., H. Saadatmanesh, and S. Tao, *Bond of Hooked GFRP Rebars to Concrete.* Materials Journal, 1995. **92**(4).

[20] EN ISO 527-1, *Plastics - Determination of tensile properties* in *Part 1: General principles*. 2012, International Organization for Standardization: Geneva, Switzerland.

[21] EN ISO 527-5, *Plastics - Determination of tensile properties* in *Part 5: Test conditions for unidirectional fibre-reinforced plastic composites*. 2009, International Organization for Standardization: Geneva, Switzerland.

[22] CSA S806, *Design and Construction of Buildings Components with Fiber-Reinforced Polymers*. 2012, Canadian Standard Association: Toronto, Ontario, Canada.

[23] Ueda, T., Y. Sato, Y. Kakuta, A. Imamura, and H. Kanematsu, *Failure Criteria for FRP Rods Subjected to a Combination of Tensile and Shear Forces*, in *Non-Metallic (FRP) Reinforcement for Concrete Structures: Proceedings of the Second International RILEM Symposium*, L. Tarwe, Editor. 1995: Ghent, Belgium.

[24] Ishihara, K., T. Obara, Y. Sato, T. Ueda, and Y. Kakuta, 1997, *Evaluation of ultimate strength of FRP rods at bent-up portion*, in *3rd Int. Symp. on Nonmetallic (FRP) Reinforcement for Concrete Structures (Vol. 2)*. 1997, Japan Concrete Institute: Sapporo, Japan. p. 27-34.

[25] Harris, B., *Engineering composite materials*. 1986: Institute of metals London.

[26] Ibell, T., A. Darby, and S. Denton, *Research issues related to the appropriate use of FRP in concrete structures.* Construction and Building Materials, 2009. **23**(4): p. 1521-1528.

[27] Hinkley, D.V., *On the ratio of two correlated normal random variables.* Biometrika, 1969. **56**(3): p. 635-639.

513 **List of Tables**

514 **Table 1. Material Properties**

Property	Carbon Fibre tow (x_f)	Epoxy Resin (x_r)	W-FRP (x_{WFRP})
Commercial Name	C T50-4.0/240-E100	Fyfe S	
Density (ρ , kg/m^3)	1800	1100	1415
Area per layer (A , mm^2)	1.92	2.35	4.28
Volume Fraction (VF)	0.45	0.55	1.00
Tensile Strength (f_u , MPa)	4000	72	1800
Tensile Modulus (E , GPa)	240.0	3.2	109.8
Elongation at break (ε_u , %)	1.7	5.0	1.64

515

516 **Table 2. Cross sectional properties of the reinforcement and test program**

517 **overview.**

	1 layer	2 layers	3 layers	4 layers	5 layers	6 layers
A_{WFRP}, mm^2	4.3	8.6	12.8	17.1	21.4	25.7
t_{WFRP}, mm	0.7	1.0	1.3	1.6	1.9	2.2
w_{WFRP}, mm	6.1	8.6	9.9	10.7	11.3	11.7
w_{WFRP}/t_{WFRP}	8.7	8.6	7.6	6.7	5.9	5.3
d_b, mm	2.3	3.3	4.0	4.7	5.2	5.7
d_{fi}, mm	0.8	1.1	1.5	1.8	2.1	2.5
ID (# repeats)	T1 (3)	T2 (3)	T3 (3)	T4 (3)	T5 (3)	T6 (3)
ID (# repeats)	L1 (5)	L2 (5)	L3 (5)	L4 (5)	L5 (5)	L6 (5)

518

519

520

521 **Table 3. Results of tensile tests**

Set of Specimens	Statistics	25 % Failure Load		50 % Failure Load		100 % Failure Load		E_{WFRP}, GPa	f_u, MPa
		$F_{25\%}$, kN	$\varepsilon_{25\%}$, %	$F_{50\%}$, kN	$\varepsilon_{50\%}$, %	F_u, kN	ε_u, %		
T1 (3 specimens)	Mean (μ)	1.65	0.372	3.29	0.723	6.58	1.404	109.47	1537
	SD	0.06	0.001	0.12	0.010	0.24	0.039	1.12	57
	CoV, %	3.7%	0.2%	3.7%	1.4%	3.7%	2.8%	1.0%	3.7%
T2 (3 specimens)	Mean (μ)	3.22	0.356	6.43	0.701	12.87	1.383	108.67	1503
	SD	0.17	0.032	0.33	0.049	0.67	0.069	2.34	78
	CoV, %	5.2%	9.1%	5.2%	7.0%	5.2%	5.0%	2.2%	5.2%
T3 (3 specimens)	Mean (μ)	4.77	0.371	9.53	0.715	19.06	1.379	107.72	1484
	SD	0.17	0.026	0.34	0.041	0.67	0.077	2.19	52.41
	CoV, %	3.5%	6.9%	3.5%	5.7%	3.5%	5.6%	2.0%	3.5%
T4 (3 specimens)	Mean (μ)	6.36	0.371	12.72	0.718	25.45	1.387	107.13	1487
	SD	0.21	0.020	0.42	0.028	0.85	0.039	0.62	49.60
	CoV, %	3.3%	5.4%	3.3%	3.9%	3.3%	2.8%	0.6%	3.3%
T5 (3 specimens)	Mean (μ)	7.63	0.351	15.26	0.686	30.52	1.339	106.57	1426
	SD	0.56	0.031	1.13	0.056	2.26	0.104	1.35	105
	CoV, %	7.4%	8.7%	7.4%	8.1%	7.4%	7.8%	1.3%	7.4%
T6 (3 specimens)	Mean (μ)	8.88	0.369	17.76	0.695	35.53	1.308	105.79	1384
	SD	0.44	0.019	0.88	0.027	1.75	0.058	0.79	68
	CoV, %	4.9%	5.1%	4.9%	3.9%	4.9%	4.5%	0.7%	4.9%

522

523

524

525

526

527

528

529

530 **Table 4. Results of bent corners tests**

Set of Specimens	Statistics	Failure load	Strains at Failure		Recorded strain signals	
		$F_{u,b}$, kN	$\varepsilon_{u,b,ave}$, %	$\varepsilon_{u,b,\max}$, %	$\varepsilon_{u,A}$, #	$\varepsilon_{u,B}$, #
L1 (5 specimens)	Mean (μ)	8.19	0.891	0.942		
	SD	0.71	0.085	0.198	4	4
	CoV, %	8.7%	9.6%	21.0%		
L2 (5 specimens)	Mean (μ)	12.76	0.903 (4)	0.955		
	SD	0.88	0.210	0.125	4	5
	CoV, %	6.9%	23.2%	13.1%		
L3 (5 specimens)	Mean (μ)	18.38	1.055 (4)	1.099		
	SD	0.68	0.133	0.120	5	4
	CoV, %	3.7%	12.6%	10.9%		
L4 (5 specimens)	Mean (μ)	23.82	0.843	0.880		
	SD	0.93	0.056	0.062	5	5
	CoV, %	3.9%	6.6%	7.1%		
L5 (5 specimens)	Mean (μ)	28.02	0.766 (4)	0.792		
	SD	1.14	0.100	0.123	5	4
	CoV, %	4.1%	13.1%	15.5%		
L6 (5 specimens)	Mean (μ)	32.02	0.534 (3)	0.540		
	SD	3.58	0.047	0.050	5	3
	CoV, %	11.2%	8.7%	9.3%		

531

532

533

534

535

536

537

538

539

540

541 **Table 5. Bent corners to straight reinforcement strength**

Number of Layers	Statistics	Exp.	f_b/f_u ACI 440 (2015)	Lee et al. (2014)	Efficiency decrease (Exp.)
1	Mean (μ)	0.622	0.407	0.597	-
	SD	0.059			
	CoV, %	9.4%			
2	Mean (μ)	0.496	0.376	0.559	-26%
	SD	0.043			
	CoV, %	8.6%			
3	Mean (μ)	0.482	0.362	0.538	-29%
	SD	0.025			
	CoV, %	5.1%			
4	Mean (μ)	0.468	0.354	0.525	-33%
	SD	0.024			
	CoV, %	5.1%			
5	Mean (μ)	0.459	0.348	0.517	-36%
	SD(μ)	0.039			
	CoV, %	8.4%			
6	Mean	0.45	0.344	0.510	-38%
	SD	0.055			
	CoV, %	12.2%			

542

543 **List of Figures**

544

545 Figure 1: Filament Wound FRP (W-FRP) reinforcement.

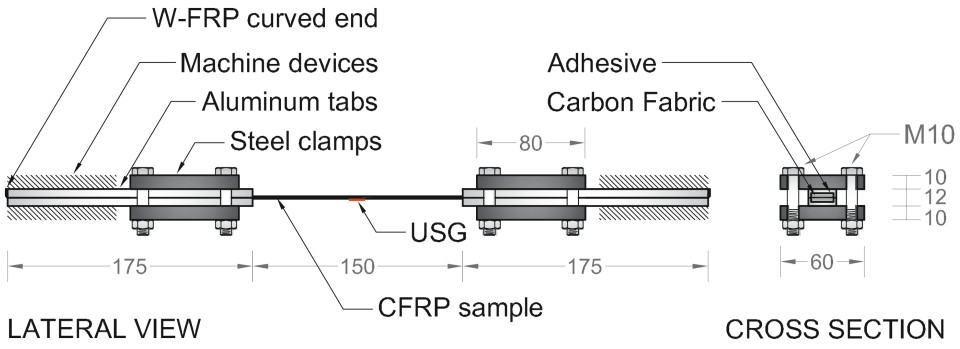

546

547 Figure 2: Tensile tests (series T) set-up.

548

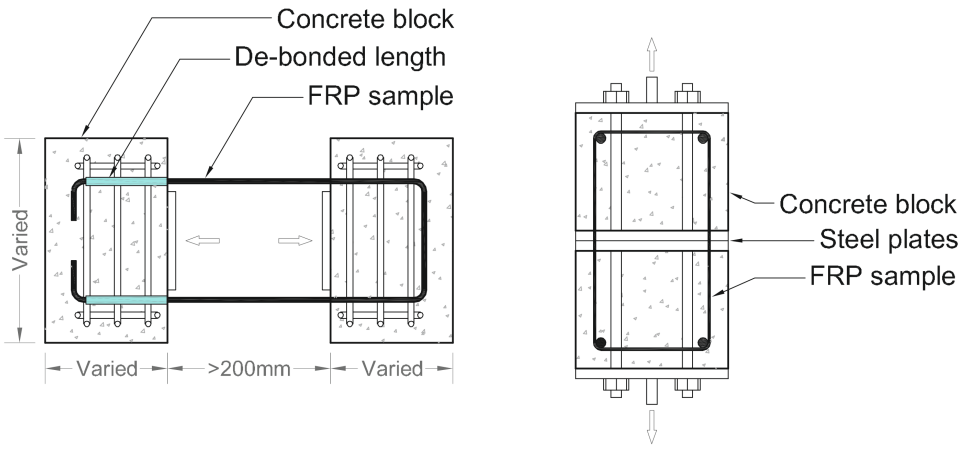

549 Figure 3. Bend strength tests set-up: a) ACI 440.3R-04; b) Ueda *et al.* [1] and Ishihara

550 *et al.* [2].

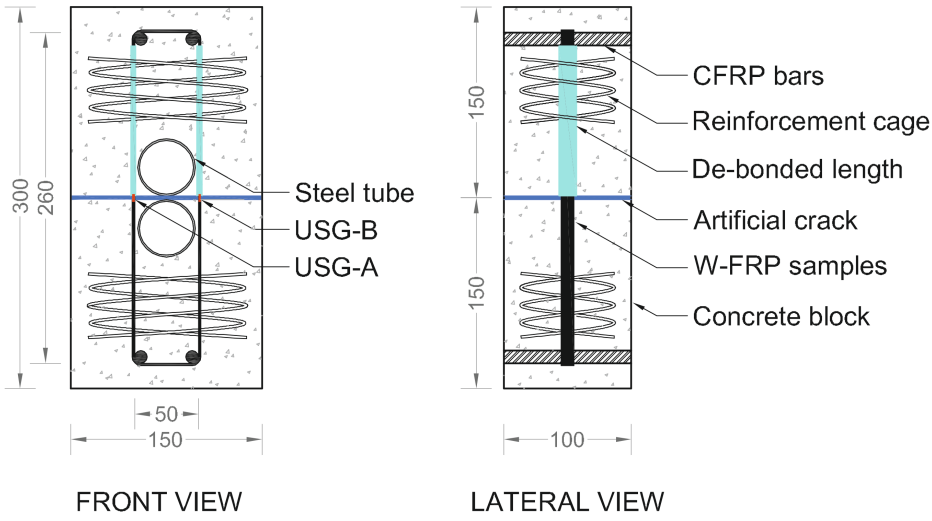

551

552 Figure 4. Samples details (Series L) - dimensions in mm.

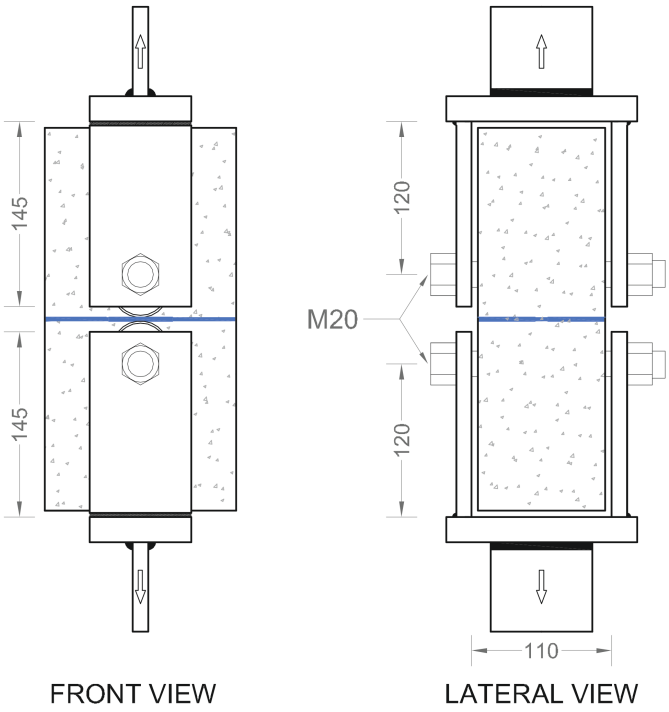

553

554 Figure 5. Loading clamp set-up - dimensions in mm.

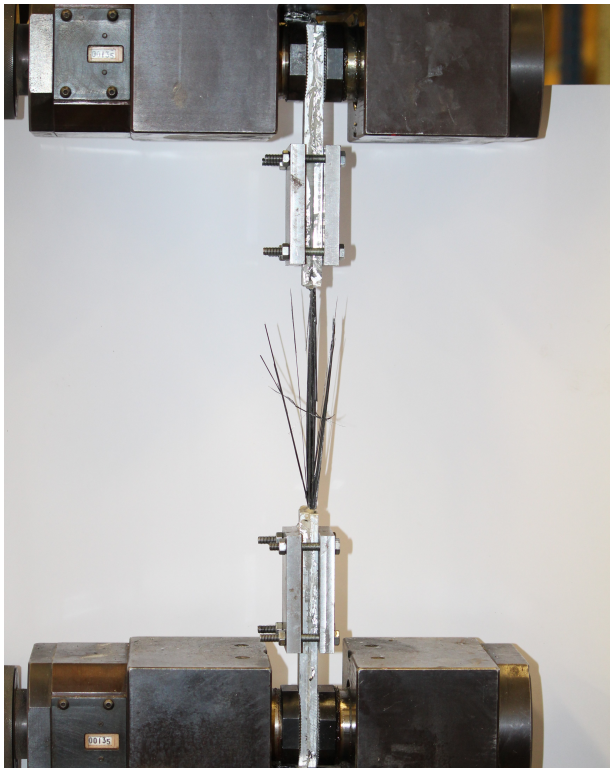

555

556 Figure 6. Specimen T5.2 at failure.

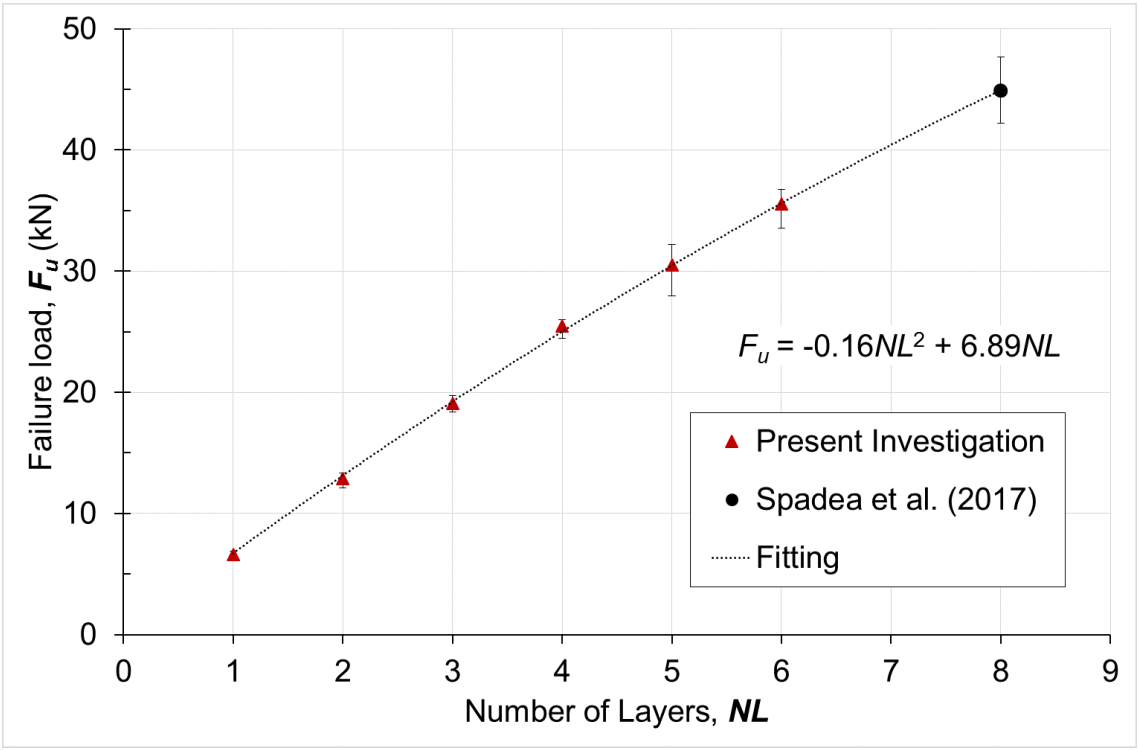

Figure 7. Failure load vs. number of layers (tensile tests).

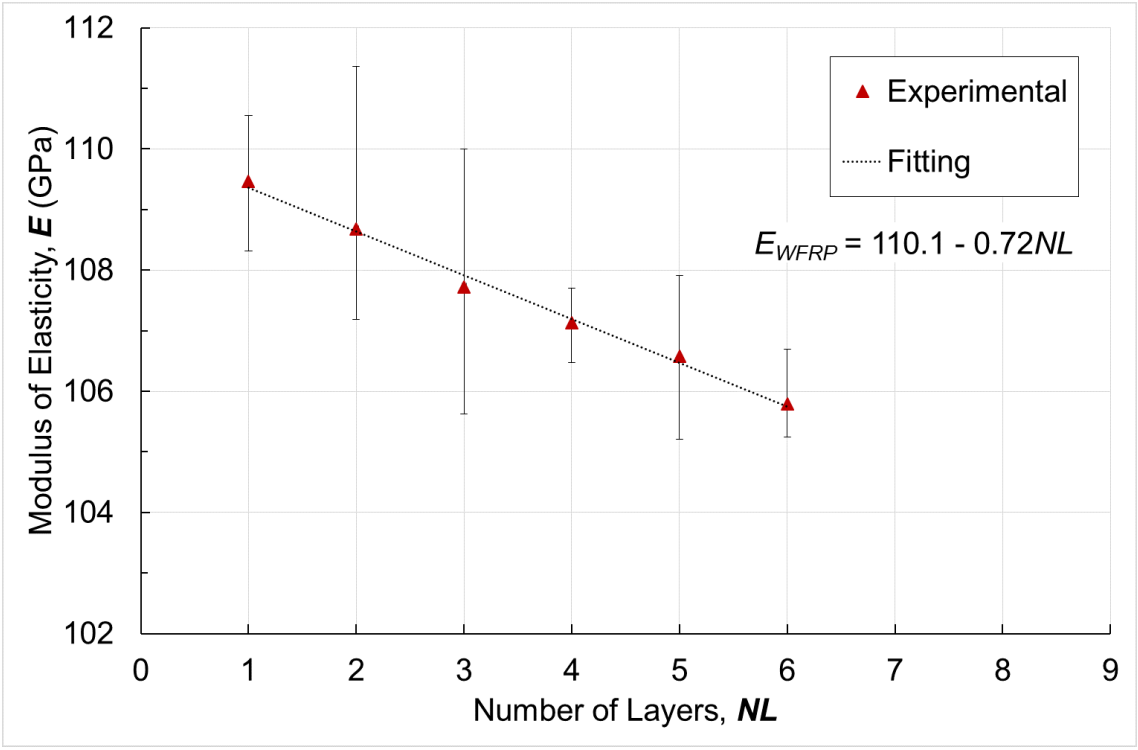

Figure 8. Modulus of elasticity vs. number of layers.

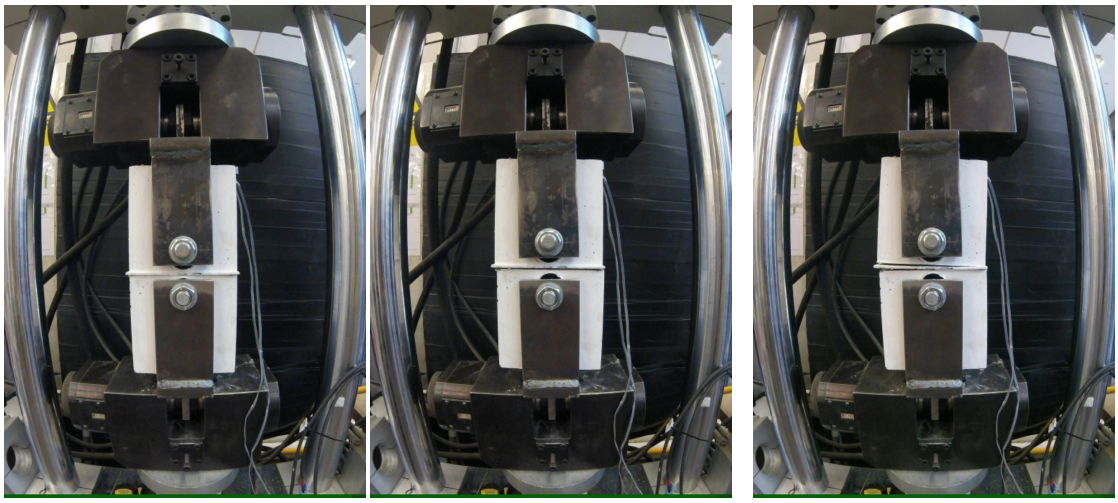

(a) (b) (c)

561 Figure 9. Time lapse of loading to failure – specimen L3.1: a) pre-loading (0.3kN, 0

562 sec); b) pre-failure (17kN, 608 sec); c) post-failure (0.4kN, 610 sec).

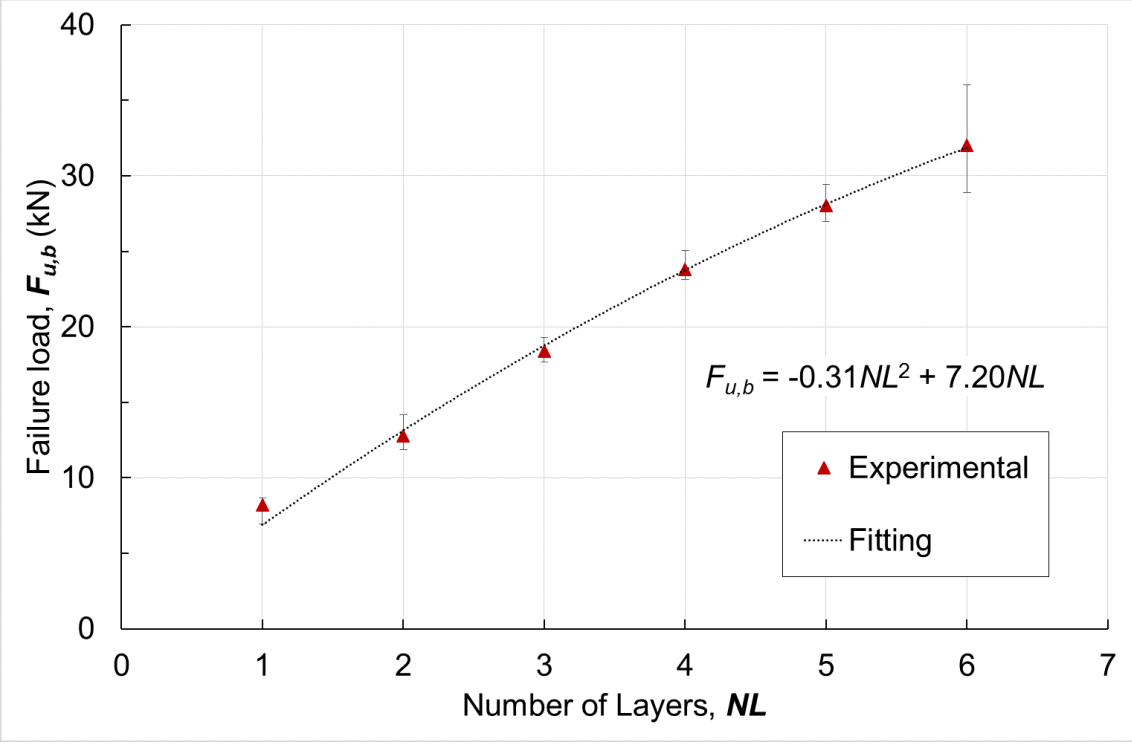

563

564 Figure 10. Failure load vs. number of layers (push off tests).

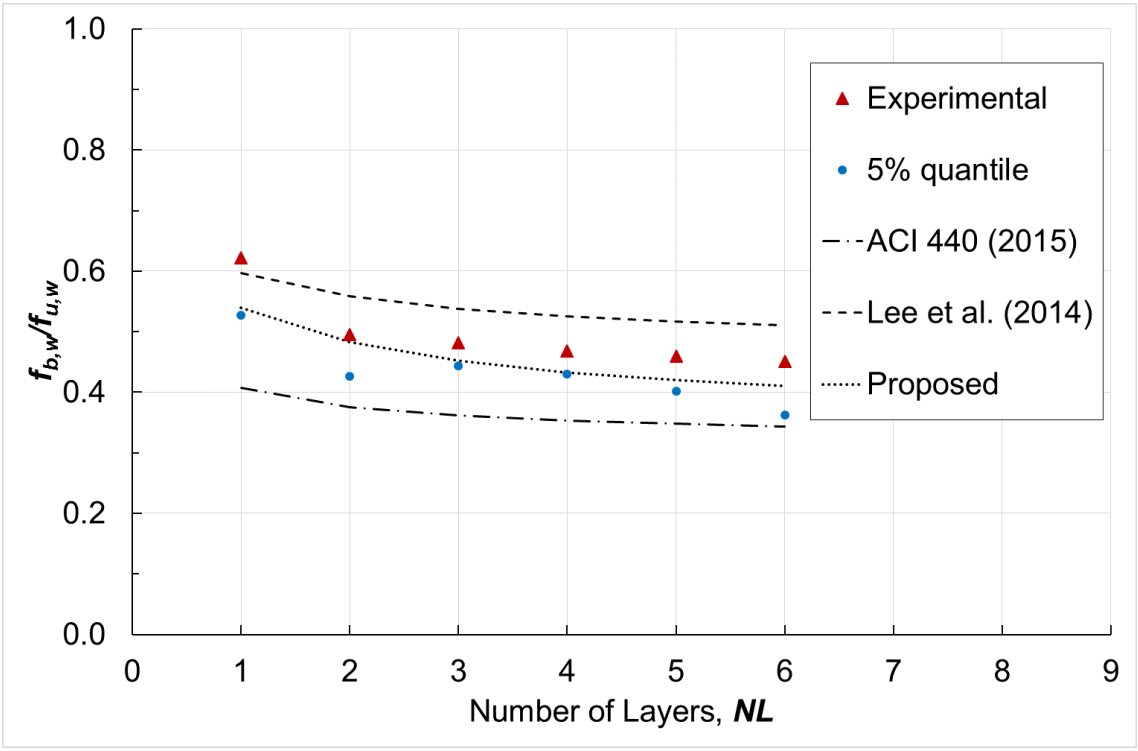

565

566 Figure 11. Bend strength to ultimate tensile strength ratios vs. number of layers.

567